International Journal of Computational Methods
Vol. 13, No. 4 (2016) 1641013 (14 pages)

DOI: 10.1142/S0219876216410139

Numerical Investigations of Waves Interacting with Free Rolling Body by Modified MPS Method

Youlin Zhang, Zhenyuan Tang and Decheng Wan*

State Key Laboratory of Ocean Engineering
School of Naval Architecture, Ocean and Civil Engineering
Shanghai Jiao Tong University, Collaborative Innovation Center for Advanced Ship and Deep-Sea Exploration
Shanghai 200240, P. R. China
**dcwan@sjtu.edu.cn*

Received 29 September 2015
Accepted 20 December 2015
Published 29 February 2016

In this paper, interaction between regular waves and free roll motion of a two-dimensional (2D) floating body is investigated by our in-house meshless particle solver MLParticle-SJTU based on modified moving particle semi-implicit (MPS) method. Numerical wave tank (NWT) is developed to calculate the interaction between waves and floating body, including wave-maker module and free roll motion module. The comparison between the numerical wave elevation and analytical solution shows that the MLParticle-SJTU solver can provide acceptable accuracy of wave making. Roll motion and force acting on the floating body in waves are in good agreement with experimental results. Profiles of the wave surface surrounding floating body are presented.

Keywords: Meshless particle method; MLParticle-SJTU solver; wave floating body interaction; wave making; roll motion.

1. Introduction

In recent years, a variety of floating structures, such as ships, offshore platforms, floating-breakwater, fish-farms, floating-airports, etc., play a crucial role in coastal and ocean engineering. It is common for floating structures to suffer from loadings under waves, and responses of these structures mounted in ocean or coastal environments have significant relation to the wave impacts. The interaction between free-surface waves and floating body is one of the key aspects in ship design or offshore structure design to increase performance and efficiency.

*Corresponding author.

In the past decades, CFD has been proved to be an effective tool for wave-structure interaction problem. A wide variety of nonlinear numerical models based on the NS equations in time domain have been developed to study this problem. The finite difference method or the finite volume method (FVM) is typically used for spatial discretization. Various techniques are adopted for interface capturing, such as the level set method and the volume of fluid method. The above approaches are based on Eulerian framework and grids are necessary for spatial discretization. The main challenges of these approaches include inefficient process of grids generation for complex structure, technology of dynamic mesh for moving boundary, simulation of free surface with large deformation, etc. Fortunately, these challenges can be avoided by the meshless particle methods.

Recently, Lagrangian particle methods draw much attention of researchers and are seen as promising numerical approaches for free surface flows, such as the smoothed particle hydrodynamics (SPH) or moving particle semi-implicit (MPS) methods. Although the SPH method is originally developed for compressible flows by Monaghan [1994], it is employed to solve incompressible flow of liquid [Oger *et al.* (2006); Yang *et al.* (2012); Bouscasse *et al.* (2013); Akbari (2014)] by choosing a sufficiently high speed of sound and a much smaller size of time step. Compared to SPH method, MPS method was originally proposed by Koshizuka and Oka [1996] for incompressible flow. Pressure of fluid is computed by a semi-implicit algorithm and a relatively large size of time step can be used. Due to these features, the MPS method is more and more popular to hydrodynamic problems, such as interaction between fluid and rigid or elastic structure [Koshizuka *et al.* (1998), (2007); Suzuki *et al.* (2007); Sueyoshi *et al.*, (2008); Shibata *et al.* (2012); Lee *et al.* (2013)]. However, accurate solution is hard to obtain since the numerical unphysical pressure oscillation, and lots of researches focus on the pressure improvement of MPS method [Khayyer and Gotoh (2009), (2010), (2011), (2012); Kondo and Koshizuka (2011); Tanaka and Masunaga (2010); Ikari *et al.* (2015)]. In the present study, an MPS solver MLParticle-SJTU is used for all simulation works. Some improved schemes are used in this solver to suppress numerical unphysical pressure oscillation. These improvements include: (i) momentum conservative pressure gradient model; (ii) modified kernel function [Zhang *et al.* (2014)]; (iii) higher order Laplacian model; (iv) mixed sourced term method for Poisson equation of pressure [Tanaka and Masunaga (2010)]; (v) surface detection method based on asymmetry of neighbor particles Zhang *et al.* (2014)]. The MLParticle-SJTU was applied in many large free-surface deformation problems, such as dam breaking flow [Zhang and Wan (2011)], liquid sloshing in LNG tank [Zhang *et al.* (2012), (2014)], impinging jet flows [Tang and Wan (2015)], etc.

This paper is organized as follows: First, the MPS method for incompressible fluid is described. Numerical approach to solve the motion of floating body is introduced. Then, numerical wave tank (NWT) is developed to calculate the interaction between waves and floating body. Time history of wave propagation is measured and compared with the analytical solution to validate the accuracy of wave making.

At last, roll motion and force acting on the floating body in waves is calculated and compared with experimental results. Profiles of the wave surface surrounding floating body are also presented.

2. Numerical Scheme

2.1. *Governing equations*

Governing equations are the continuum equation and the momentum equation. These equations for incompressible viscous fluid are represented as

$$\frac{1}{\rho}\frac{D\rho}{Dt} = -\nabla \cdot \mathbf{V} = 0, \tag{1}$$

$$\frac{D\mathbf{V}}{Dt} = -\frac{1}{\rho}\nabla P + \nu\nabla^2\mathbf{V} + \mathbf{g}, \tag{2}$$

where $\mathbf{V}$ is the velocity vector, t is the time, ρ is the density, P is the pressure, ν is the kinematic viscosity and $\mathbf{g}$ is the gravity acceleration.

2.2. *Discrete expressions of particle interaction models*

2.2.1. *Kernel function*

In particle method, governing equations are transformed to the equations of particle interactions. The particle interactions are based on the kernel function. In traditional MPS method, a simple and convenient kernel function is introduced by Koshizuka as

$$W(r) = \begin{cases} \frac{r_e}{r} - 1, & 0 \le r < r_e, \\ 0, & r_e \le r, \end{cases} \tag{3}$$

where r is the particle distance and r_e is the cutoff radius. A drawback of the above kernel function is that it becomes singular at $r = 0$. This may cause unreal pressure between two neighboring particles with a small distance, and affect the computational stability. To overcome this, an improved kernel function is used in this paper [Zhang and Wan (2012)]

$$W(r) = \begin{cases} \frac{r_e}{0.85r + 0.15r_e} - 1, & 0 \le r < r_e, \\ 0, & r_e \le r. \end{cases} \tag{4}$$

The above kernel function has a similar form with the original kernel function Eq. (3), but without singularity.

2.2.2. *Gradient model*

Gradient operator is modeled as a local weighted average of the gradient vectors between particle i and its neighboring particles j

$$\langle \nabla\phi \rangle_i = \frac{D}{n^0} \sum_{j \ne i} \frac{\phi_j + \phi_i}{|\mathbf{r}_j - \mathbf{r}_i|^2} (\mathbf{r}_j - \mathbf{r}_i) \cdot W(|\mathbf{r}_j - \mathbf{r}_i|), \tag{5}$$

where ϕ is an arbitrary scalar function, D is the number of space dimensions and n^0 is the initial particle number density for incompressible flow. The particle number density in MPS method is defined as

$$\langle n\rangle_i = \sum_{j\neq i} W(|\mathbf{r}_j - \mathbf{r}_i|). \tag{6}$$

2.2.3. *Higher order Laplacian model*

In traditional MPS method, Laplacian operator is derived by Koshizuka *et al.* [1998] from the physical concept of diffusion as

$$\langle \nabla^2 \phi\rangle_i = \frac{2D}{n^0\lambda} \sum_{j\neq i} (\phi_j - \phi_i) \cdot W(|\mathbf{r}_j - \mathbf{r}_i|), \tag{7}$$

$$\lambda = \frac{\sum_{j\neq i} W(|\mathbf{r}_j - \mathbf{r}_i|) \cdot |\mathbf{r}_j - \mathbf{r}_i|^2}{\sum_{j\neq i} W(|\mathbf{r}_j - \mathbf{r}_i|)}, \tag{8}$$

where λ is a parameter, introduced to keep the variance increase equal to that of the analytical solution.

In the past few years, higher order Laplacian models have been derived to improve and stabilize the pressure calculation, such as Eq. (9) given by Khayyer and Gotoh [2010].

$$\langle \nabla^2 \phi\rangle_i = \frac{1}{n^0} \sum_{j\neq i} \left(\phi_{ij} \frac{\partial^2 w_{ij}}{\partial r_{ij}^2} - \frac{\phi_{ij}}{r_{ij}} \frac{\partial w_{ij}}{\partial r_{ij}} \right). \tag{9}$$

In this paper, the higher order Laplacian model can be written as Eq. (10) by considering the modified kernel function Eqs. (4) and (9).

$$\langle \nabla^2 \phi\rangle_i = \frac{1}{n^0} \sum_{j\neq i} \frac{2.295\phi_{ij}}{(0.85r + 0.15r_e)^3}. \tag{10}$$

2.3. *Model of incompressibility*

The incompressible condition in traditional MPS method is represented by keeping the particle number density constant. The algorithm of incompressibility model consists two stages in each time step, explicit and implicit stages. First, temporal velocity of particles is calculated based on viscous and gravitational forces, and particles are moved according to the temporal velocity. Second, pressure is implicitly calculated by solving Poisson pressure equation (PPE), the velocity and position of particles are updated according to the obtained pressure. The PPE is defined as [Koshizuka *et al.* (1998)]

$$\langle \nabla^2 P^{k+1}\rangle_i = -\frac{\rho}{\Delta t^2} \frac{\langle n^*\rangle_i - n^0}{n^0}, \tag{11}$$

where n^* is the particle number density in temporal flow field.

The source term of the Poisson equation in Eq. (11) is solely based on the deviation of the temporal particle number density from the initial value. As the particle number density field is not smooth, the pressure obtained from Eq. (11) is prone to oscillate in spatial and temporal domains. To suppress such unphysical oscillation of pressure, Tanaka and Masunaga [2010] proposed a mixed source term for PPE, which combines the velocity divergence and the particle number density. The main part of the mixed source term is the velocity divergence, while the particle number density is used to keep the fluid volume constant. This improved PPE is rewritten by Lee *et al.* [2011] as

$$\langle \nabla^2 P^{k+1} \rangle_i = (1-\gamma)\frac{\rho}{\Delta t}\nabla \cdot \mathbf{V}_i^* - \gamma \frac{\rho}{\Delta t^2}\frac{\langle n^k \rangle_i - n^0}{n^0}, \tag{12}$$

where γ is a blending parameter with a value between 0 and 1. The value of γ has large effect on the pressure field. In particular, the larger γ produces smoother pressure field. However, the volume of fluid cannot be constant while $\gamma = 0$. The effects of γ have been investigated by Tanaka and Masunaga [2010] and Lee *et al.* [2011]. $\gamma = 0.01$ is used in this paper.

2.4. *Time stepping procedures*

The procedure of MPS method is divided into two substeps for every time step. First, all terms except the pressure term in the momentum conservation equation are evaluated explicitly, and the temporal velocities and positions of particles are computed as

$$\mathbf{V}_i^* = \mathbf{V}_i^n + \Delta t(\nu \nabla^2 \mathbf{V} + \mathbf{g}), \tag{13}$$

$$\mathbf{r}_i^* = \mathbf{r}_i^k + \Delta t \cdot \mathbf{V}_i^*. \tag{14}$$

Second, the pressure term is solved implicitly according to the incompressible condition (Eq. (12)) by the bi-conjugate gradients stabilized (Bi-CGSTAB) method. Then, the velocities and positions are modified as

$$\mathbf{V}_i^{k+1} = \mathbf{V}_i^* - \frac{\Delta t}{\rho}\nabla P^{k+1}, \tag{15}$$

$$\mathbf{r}_i^{k+1} = \mathbf{r}_i^k + \Delta t \cdot \mathbf{V}_i^{k+1}. \tag{16}$$

2.5. *Free surface boundary condition*

On the surface particles, the free surface boundary conditions, including kinematic and dynamic boundary conditions, are imposed. The kinematic condition is directly satisfied in Lagrangian particle method, while the dynamic condition is implemented by setting zero pressure on the free surface particles. So the accuracy of surface particle detection has significant effect on pressure field.

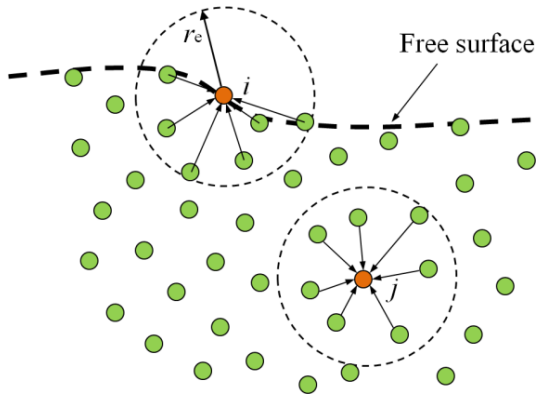

Fig. 1. Description of particle interaction domain.

The interaction domain is truncated in the free surface (Fig. 1), so the particle number density near the free surface is lower than that in the inner field. In traditional MPS method, particle satisfying [Koshizuka *et al.* (1998)]

$$\langle n\rangle_i^* < \beta\, n^0 \tag{17}$$

is considered as free surface particle, where β is a parameter, can be chosen between 0.8 and 0.99.

The traditional detection method (Eq. (17)) is based on the particle number density. However, inner particles with small particle number density may be misjudged as free surface particles, thus unreal pressure around the misjudged particles occur. This usually causes nonphysical pressure oscillation. To improve the accuracy of surface particle detection, we employ a new detection method in which a vector function is defined as [Zhang *et al.* (2014)]

$$\langle \mathbf{F}\rangle_i = \frac{D}{n^0}\sum_{j\neq i}\frac{1}{|\mathbf{r}_i - \mathbf{r}_j|}(\mathbf{r}_i - \mathbf{r}_j)W(\mathbf{r}_{ij}). \tag{18}$$

The vector function $\mathbf{F}$ represents the asymmetry of arrangements of neighbor particles.

Particle satisfying

$$\langle|\mathbf{F}|\rangle_i > \alpha \tag{19}$$

is considered as free surface particle, where α is assigned to $0.9\,|\mathbf{F}|^0$ in this paper, $|\mathbf{F}|^0$ is the initial value of $|\mathbf{F}|$ for surface particle.

It should be specially noted that Eq. (19) is only valid for particles with number density between $0.8n^0$ and $0.97n^0$ since particles with number density lower than $0.8n^0$ is definitely surface particles, while those with number density higher than $0.97n^0$ should get pressure through Poisson equation.

2.6. *Motion of floating body*

The motion of the floating body is governed by the equations of rigid body dynamics, following the Newton's law of motion. The translation motion of the center of gravity and the rotation of the rigid body are given in a simple two-dimensional (2D) framework by

$$\begin{cases} M\frac{d\mathbf{V}_G}{dt} = M\mathbf{g} + \mathbf{F}_{\text{fluid}-\text{solid}}, \\ I_G\frac{d\mathbf{\Omega}_G}{dt} = \mathbf{T}_{\text{fluid}-\text{solid}}, \end{cases} \tag{20}$$

where M and I_G are the mass and the moment of inertia of the floating body around the center of gravity, respectively. $\mathbf{V_G}$ and $\mathbf{\Omega}_G$ are the linear velocity of the center of gravity and the angular velocity of the body, respectively. $\mathbf{F}_{\text{fluid}-\text{solid}}$ is the hydrodynamic force acting on the body and $\mathbf{T}_{\text{fluid}-\text{solid}}$ is the hydrodynamic torque with the direction normal to the plane.

3. Numerical Simulations

In this study, three 2D computations are investigated to evaluate the performance of our in-house particle solver based on modified MPS method. First, damped roll motion of a floating box is studied and compared with previous experimental study performed by Jung [2004]. Then, an NWT is developed and the accuracy of wave making is investigated. Besides, wave floating body interaction problems are studied.

3.1. *Validation of damped roll motion*

In this section, the damped motion of a floating box is studied to verify the simulation of a floating body with free surface. The initial geometry and setup are shown in Fig. 2. The width and height of the rectangular floating body are 0.3 m and 0.1 m, respectively. The box is installed at the symmetrical axis and 0.4 m above the bottom of tank, fixed at the center of its gravity but free in the degree of roll, inclined with the initial angle $\theta = 15°$. Mass moment of inertia of the box is $0.36\,\text{kg}\cdot\text{m}^2$. Density of water is $1{,}000\,\text{kg/m}^3$. Water tank filled with particles of different spatial resolution (0.01, 0.004 and 0.002 m) is simulated to check the convergence of the numerical model. The cutoff radius r_e is 2.3 for all cases in this paper. One core was used on the personal computer (Intel Core $^{\text{TM}}$i7-4790 K at 4 GHz) for all the three cases.

Since reflex waves generated by the oscillation of box should be avoided to obtain accurate roll angles, sponge layers are placed at both sides of the water tank. In sponge layer, artificial damping term $-\phi(x)\mathbf{V}$ is introduced to left-hand side of Eq. (2) for absorption of waves and defined as

$$\phi(x) = \begin{cases} 0 & \text{out of sponge layer}, \\ \delta\frac{|x-x_0|}{l} & \text{in sponge layer}, \end{cases} \tag{21}$$

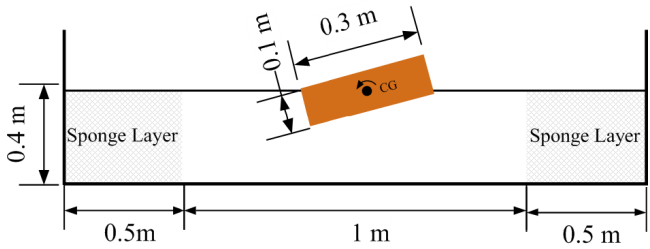

Fig. 2. Sketch of damped roll motion.

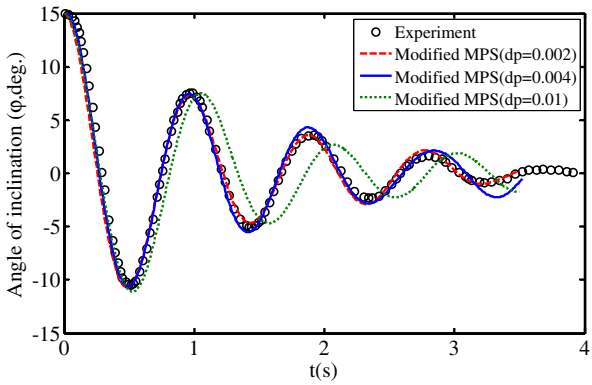

Fig. 3. Time history of roll angle during the damped rolling oscillation (dp is the initial distance between particles).

where δ is coefficient for controlling the intensity of the sponge layer, l is width of sponger layer and x_0 is the horizontal position where waves initially enter into the damping layer.

Figure 3 shows the comparison of the time history of roll angles between the computed results with different spatial resolutions and the experimental data. The cycle points represent roll angles obtained by Jung's experiment. The roll motion decays after each period by the damping effect. For the case dp = 0.01 m, period of roll motion is much different from that of experimental data. For the cases dp = 0.004 m and dp = 0.002 m, both period and amplitude of roll motion agree very well comparing to experimental data. The time costs for 5,000 computational steps are 4, 55 and 342 min, corresponding to the cases dp = 0.01, dp = 0.004 and dp = 0.002. Considering the computational efficiency, initial distance between fluid particles is set to be 0.004 m for all other simulations presented in this paper.

3.2. *Validation of wave making*

In this work, numerical wave elevation is investigated to verify the accuracy of wave generation. Sketch of the numerical setup is shown in Fig. 4 but without floating

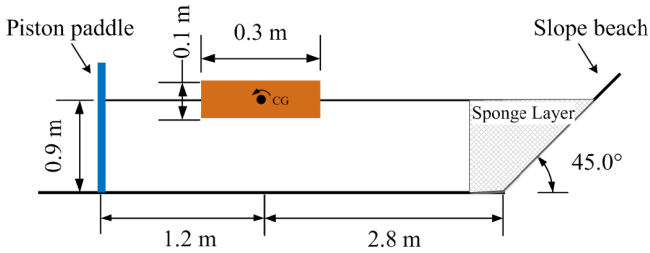

Fig. 4. Sketch of the 2D wave tank.

Table 1. Parameters of wave making.

Parameters	Values
Water density	1,000 (kg/m^3)
Water height	0.9 (m)
Wave length	1 (m)
Wave height	0.029
Wave period	0.8 (s)
Fluid spacing	0.004 (m)
No. of fluid particles	132,750
No. of total particles	138,130

box in the tank. A piston-type wave generator is incorporated in the left side of 2D NWT. Sponge layer and a slop beach is installed at the end of the wave tank to absorb waves and avoid reflection. The NWT is of 5.5 m width and 1.5 m height with initial water depth 0.9 m. Wave conditions used in present numerical test are shown in Table 1, and traveling waves are generated based on linear wave theory.

Figure 5 shows a comparison between numerical wave elevation and analytical solution at the location 1.05 m from the initial position of piston paddle where a floating box will be placed in the next section. The numerical data is represented by solid line and be smoothed within 0.01 s. The trend of numerical free surface height is in agreement with the analytical solution.

3.3. *Validation of motion of freely rolling body in waves*

As presented in previous sections, the NWT-based modified MPS method can be employed to deal with problems such as damped roll motion of floating box and wave making successfully. In this section, interactions between floating box and waves are investigated in time domain to verify the accuracy of the computed roll motion and wave forces. All the initial geometry and set-up are same as shown in Fig. 4.

In the present simulation, the distance between particles is 0.004 m, the total number of particles is 137,718, while the number of fluid particles is 131,762. The gravitational acceleration and water density are 9.8 m/s^2 and 1,000 kg/m^3. The

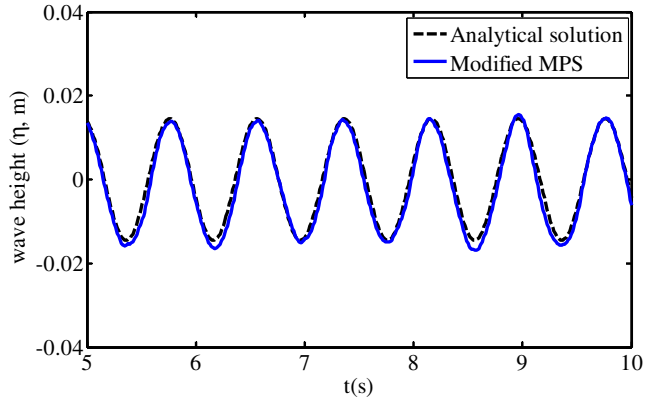

Fig. 5. Comparison between numerical wave elevation and analytical solution (solid line: smoothed result of simulation; dashed line: result of linear wave theory).

kinematic viscosity of water is given by $1.01 \times 10^{-6}\,\mathrm{m}^2/\mathrm{s}$. The time step size is 0.0004 s and the total computational time is 10 s. Waves with period of 0.8 s were generated in this study. The wave conditions used in the present computation are same as shown in Table 1.

In the free rolling simulation of rectangular structure, angles of roll motion about the center of gravity were measured when the regular roll motion of rectangular body can be obtained.

Figure 6 shows the inclined angle of the floating box over one period of the regular wave. Results about the roll motion of the structure is compared between present simulation and experiment by Jung [2004]. It can be found that both the pattern of curves and amplitude of roll angles are in good agreement.

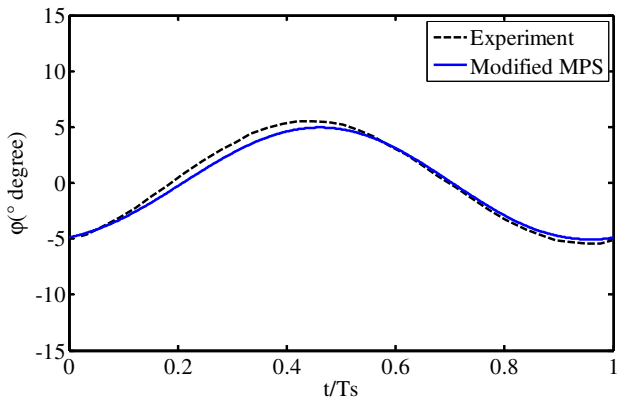

Fig. 6. Rolling motion of the rectangular body within wave period (solid line: result of simulation; dashed line: result of Jung [2004]).

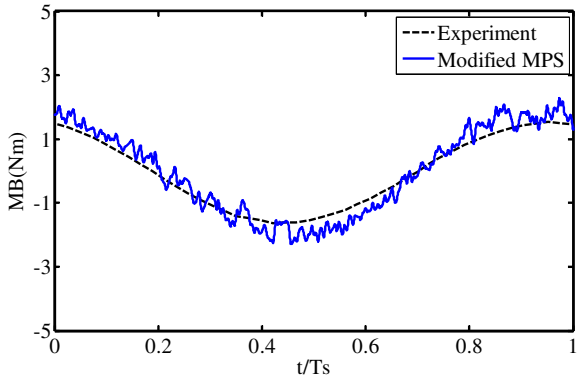

Fig. 7. Time history of buoyancy restoring moment of the rectangular body within wave period (solid line: result of simulation; dashed line: result of Jung [2004]).

Details about buoyancy restoring moment (M_B, moment of the surface forces about the gravitational center of the rectangular structure) of the freely rolling body should be noteworthy, since the roll motion is closely related with the change of M_B in time domain. Figure 7 shows the time history of buoyancy restoring moment in one wave period. It can be seen that the calculated results of M_B agree fairly well with experimental results. Though several improvements have been employed in present solver, the numerical unphysical pressure oscillation is hard to eliminate completely, and this induces the fluctuation of restoring moment.

Figure 8 shows the evolution process of rotation of the floating body. It can be seen that positions of the floating box is strong influenced by the propagation of

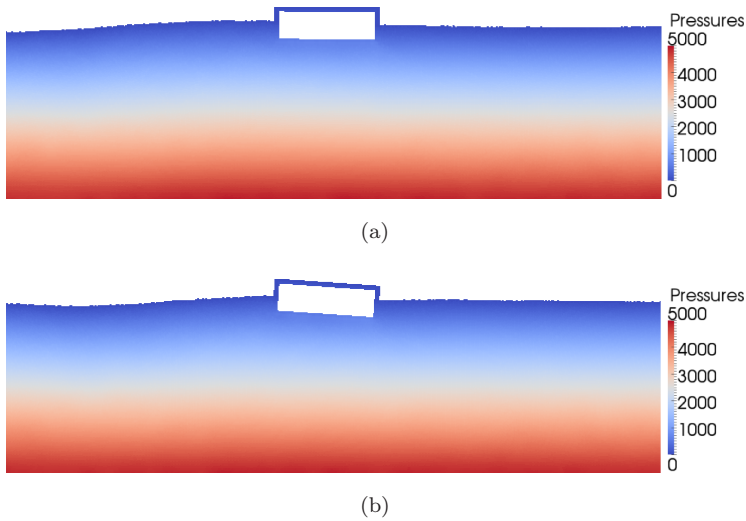

Fig. 8. Rotary positions and wave surfaces around floating box. (a) $t = t_0$, (b) $t = t_0 + T/4$, (c) $t = t_0 + T/2$, (d) $t = t_0 + 3T/4$ and (e) $t = t_0 + T$.

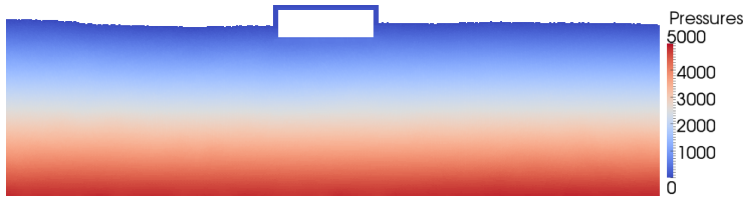

(c)

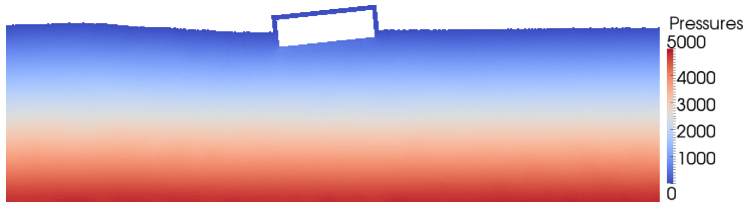

(d)

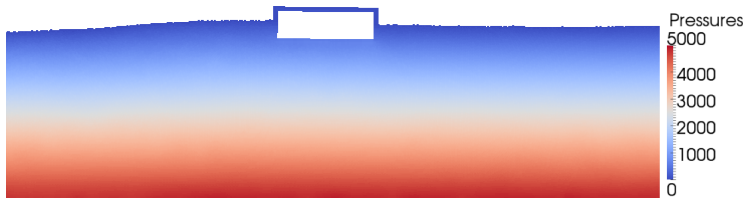

(e)

Fig. 8. (*Continued*)

incident wave through five snapshots of representative instants ($t_0, t_0 + T/4, t_0 + T/2, t_0 + 3T/4$ and $t_0 + T$) in a wave period. First, the body rotates clockwise until the value of M_B climbs up to the maximum with the coming wave from left. After that, the crest of the wave transfers from left to right of the floating box. At the same time, buoyancy restoring moment of the body decreases. As a result, box rotates anticlockwise and returns to horizontality at the instant of $t_0 + T/2$. With the propagating of the wave, water surface falls on the left and rises on the right from $t_0 + T/2$ to $t_0 + 3T/4$. Box keeps on rotating anticlockwise until the value of M_B declines to the minimum. Form the instant of $t_0 + 3T/4$, it begins to rotate clockwise again, and returns to nearly horizontality at $t_0 + T$ finally. The rotation of floating body will repeat with the next wave coming from left.

4. Conclusion

In this paper, interaction between regular waves and free roll motion of a 2D floating body is investigated by our in-house particle solver MLParticle-SJTU based on

modified MPS method. Five improvements, including nonsingular kernel function, momentum conservative pressure gradient model, higher order Laplacian model, mixed source term for PPE and an accurate surface detection method, are employed in this solver. NWT is developed to calculate the interaction between waves and floating body, including wave-maker module and free roll motion module. The comparison between the numerical wave elevation and analytical solution shows that the MLParticle-SJTU can provide acceptable accuracy of wave making. Numerical roll motion and force acting on the floating body in waves are in good agreement with the experimental results. At last, the evolution process of rotation of the floating body was shown through five snapshots of representative-instants ($t_0, t_0 + T/4, t_0 + T/2, t_0 + 3T/4$ and $t_0 + T$) in a wave period. It can be seen that positions of the floating box are strongly influenced by the propagation of incident wave. According to the results present in previous sections, the solver can be used to deal with wave floating body interaction problems.

Acknowledgments

This work is supported by National Natural Science Foundation of China (Grant Nos. 51379125, 51490675, 11432009 and 51411130131), The National Key Basic Research Development Plan (973 Plan) Project of China (Grant No. 2013CB036103), High Technology of Marine Research Project of The Ministry of Industry and Information Technology of China, Chang Jiang Scholars Program (Grant No. T2014099) and the Program for Professor of Special Appointment (Eastern Scholar) at Shanghai Institutions of Higher Learning (Grant No. 2013022), to which the authors are most grateful.

References

Akbari, H. [2014] "Modified moving particle method for modeling wave interaction with multilayered porous structures," *Coast. Eng.* **89**, 1–19.

Bouscasse, B., Colagrossi, A., Marrone, S. and Antuono, M. [2013] "Nonlinear water wave interaction with floating bodies in SPH," *J. Fluids Struct.* **42**, 112–129.

Ikari, H., Khayyer, A. and Gotoh, H. [2015] "Corrected higher order Laplacian for enhancement of pressure calculation by projection-based particle methods with applications in ocean engineering," *J. Ocean Eng. Mar. Energy* **1**, 361–376.

Jung, K. H. [2004] *Experimental study on rectangular barge in beam sea*, Ph.D. Thesis, Texas A&M University, Texas.

Khayyer, A. and Gotoh, H. [2009] "Modified moving particle semi-implicit methods for the prediction of 2D wave impact pressure," *Coast. Eng.* **56**, 419–440.

Khayyer, A. and Gotoh, H. [2010] "A higher order Laplacian model for enhancement and stabilization of pressure calculation by the MPS method," *Appl. Ocean Res.* **32**, 124–131.

Khayyer, A. and Gotoh, H. [2011] "Enhancement of stability and accuracy of the moving particle semi-implicit method," *J. Comput. Phys.* **230**, 3093–3118.

Khayyer, A. and Gotoh, H. [2012] "A 3D higher order Laplacian model for enhancement and stabilization of pressure calculation in 3D MPS-based simulations," *Appl. Ocean Res.* **37**, 120–126.

Kondo, M. and Koshizuka, S. [2011] "Improvement of stability in moving particle semi-implicit method," *Int. J. Numer. Methods Fluids* **65**, 638–654.

Koshizuka, S. and Oka, Y. [1996] "Moving-particle semi-implicit method for fragmentation of incompressible fluid," *Nucl. Sci. Eng.* **123**, 421–434.

Koshizuka, S., Obe, A. and Oka, Y. [1998] "Numerical analysis of breaking waves using the moving particle semi-implicit method," *Int. J. Numer. Methods Fluids* **26**, 751–769.

Koshizuka, S., Shibata, K., Tanaka, M. and Suzuki, Y. [2007] 'Numerical analysis of fluid-structure and fluid-rigid body interactions using a particle method," *Proc. FEDSM2007*, San Diego, California, USA, pp 177–182.

Lee, B. H., Park, J. C., Kim, M. H. and Hwang, S. C. [2011] "Step-by-step improvement of MPS method in simulating violent free-surface motions and impact-loads," *Comput. Methods Appl. Mech. Eng.* **200**, 1113–1125.

Lee, B. H., Jeong, S. M., Hwang, S. C., Park, J. C. and Kim, M. H. [2013] "A particle simulation of 2-D vessel motions interacting with liquid-sloshing cargo," *Comput. Model. Eng. Sci.* **91**, 43–63.

Monaghan, J. J. [1994] "Simulating free surface flows with SPH," *J. Comput. Phys.* **110**, 399–406.

Oger, G., Doring, M., Alessandrini, B. and Ferrant, P. [2006] "Two-dimensional SPH simulations of wedge water entries," *J. Comput. Phys.* **213**, 803–822.

Shibata, K., Koshizuka, S., Sakai, M. and Tanizawa, K. [2012] "Lagrangian simulations of ship-wave interactions in rough seas," *Ocean Eng.* **42**, 13–25.

Sueyoshi, M., Kashiwagi, M. and Naito, S. [2008] "Numerical simulation of wave-induced nonlinear motions of a two-dimensional floating body by the moving particle semi-implicit method," *J. Mar. Sci. Technol.* **13**, 85–94.

Suzuki, Y., Koshizuka, S. and Oka, Y. [2007] "Hamiltonian moving-particle semi-implicit (HMPS) method for incompressible fluid flows," *Comput. Methods Appl. Mech. Eng.* **196**, 2876–2894.

Tanaka, M. and Masunaga, T. [2010] "Stabilization and smoothing of pressure in MPS method by Quasi-Compressibility," *J. Comput. Phys.* **229**, 4279–4290.

Tang, Z. Y. and Wan, D. C. [2015] "Numerical simulation of impinging jet flows by modified MPS method," *Eng. Comput.* **32**(4), 1153–1171.

Yang, Q., Jones, V. and McCue, L. [2012] "Free-surface flow interactions with deformable structures using an SPH–FEM model," *Ocean Eng.* **55**, 136–147.

Zhang, Y. X. and Wan, D. C. [2011] "Application of MPS in 3D dam breaking flows," *Sci. China Phys. Mech. Astron.* **41**, 140–154.

Zhang, Y. X. and Wan, D. C. [2012] "Apply MPS method to simulate liquid sloshing in LNG tank," *Proc. 22nd Int. Offshore and Polar Engineering Conf.*, Rhodes, Greece, pp. 381–391.

Zhang, Y. X., Wan, D. C. and Hino, T. [2014] "Comparative study of MPS method and level-set method for sloshing flows," *J. Hydrodyn.* **26**(4), 577–585.